JOURNAL OF GEOPHYSICAL RESEARCH, VOL. 102, NO. C5, PAGES 10,585–10,602, MAY 15, 1997

Inferring meridional mass and heat transports of the Indian Ocean by fitting a general circulation model to climatological data

Tong Lee
Jet Propulsion Laboratory, California Institute of Technology, Pasadena

Jochem Marotzke
Center for Global Change Science, Massachusetts Institute of Technology, Cambridge

Abstract. The meridional overturning and heat transport of the Indian Ocean are studied by fitting the steady state dynamics of a general circulation model (GCM) to climatological annual mean temperatures, salinities, and surface forcings using the GCM and its adjoint. By estimating target temperatures and salinities near the artificially closed side boundaries as part of the optimization procedure, a steady solution that is consistent with climatological data within limits of observational errors is found. The resultant meridional overturning is vigorous (14 Sv; 1 Sv = 10^6 m^3/s) only in the upper 1000 m. The estimated deep inflow entering the Indian Ocean from the south is weak. Requiring a large net northward inflow at depth does not result in strong interior upwelling but leads to unrealistically large baroclinic mass exchange and implied vertical mixing near the Indonesian throughflow region. The shallow overturning is the main carrier of the southward heat transport, which has a maximum of 0.8 PW (1 PW = 10^{15} W) near 15°S. Wind forcing plays a key role in driving the estimated overturning of the Indian Ocean. This result is in disagreement with previous interpretations about the central role of surface heat flux in driving a vigorous deep overturning of the Indian Ocean.

1. Introduction

Climatological surface heat flux data [*Oberhuber*, 1988] indicate that the Indian Ocean receives a net heat input from the atmosphere upon annual average. Since this ocean is closed to the north at low latitudes, the net heat gain has to be carried to the south to maintain balance. This can be achieved by meridional mass overturning with net southward transport of warmer waters replenished by net upwelling and northward transport of colder waters. The strength and structure of this overturning and the meridional heat flux associated with it, however, are poorly understood.

Previous studies of the meridional overturning and heat transport of the Indian Ocean fall into three categories of combining data with dynamics. The first type is geostrophic calculation using cross-basin hydrographic sections with assumed levels of no motion (LNM). An example is *Toole and Warren* [1993], based on a densely sampled hydrographic section near 32°S. This study suggests a vigorous deep overturning of the Indian Ocean with 27 Sv of net northward transport below 2000 m (the uncertainty of the estimate was said to be about 30%). In steady state this deep inflow implies a mean upwelling rate across the 2000-m level (north of 32°S) of 6.9 × 10^{-5} cm/s, several times larger than in the Pacific (at the same level). Furthermore, it was suggested that net deep northward flow resulted from the difference in transport between strong Deep Western Boundary Currents (DWBCs) along several ridges (the Madagascar Ridge, Central Indian Ridge, and Ninetyeast Ridge) and weaker horizontal return flows in the broad interior. In contrast, *Toole and Raymer* [1985] obtained a much smaller net northward transport at depth based on a sparsely sampled section near 32°S. It is important to appreciate that the result obtained from geostrophic calculation is an interpretation of the hydrographic data based on an assumed level of no motion (LNM) rather than a direct observation. In the study by *Toole and Warren* [1993] the LNM is chosen through an analysis of water property boundaries and by maximizing northward transport at depth. Potential bias is incurred because (1) water property distribution is largely set by long-term flow and therefore could be decoupled from an instantaneous velocity field and (2) boundaries between water masses are sometimes not very distinguishable in the interior due to mixing.

The second type of study used the linear inversion technique put forth by *Wunsch* [1978], which combined hydrography-based geostrophic calculation with conservation laws of mass, salt, and/or tracer to estimate velocities across each section. Examples are *Fu*'s [1986] inversion for the southern Indian Ocean and *Macdonald*'s [1995] global inversion. The corresponding estimates of net northward flow near 32°S below 2000 m are 3.5 and 16 Sv. In a recent study, *Robbins and Toole* [1997] reanalyzed the 32°S section using the linear inversion technique and using silica conservation as a constraint to the choice of LNM. They obtained a new estimate of 10 Sv as opposed to 27 Sv by *Toole and Warren* [1993]. To what degree the results of linear inversions are subject to bias in the initial choice of LNM is somewhat uncertain. *Robbins and Toole* [1997] obtained an uncertainty of 3 Sv through a Monte Carlo experiment in which the initial choices of LNM are randomly perturbed by ±500 m.

Paper number 97JC00464.
0148-0227/97/97JC-00464$09.00

The third type of studies is simulation using general circulation models (GCMs) (few of which have been applied to this problem). Examples are eddy-resolving global [*Semtner and Chervin*, 1992] and Indian Ocean [*Wacongne and Pacanowski*, 1996] GCMs. Both simulations show little net northward flow at depth. Neither study examines the driving force of the overturning explicitly. These models are constrained by hydrographic data only through relaxation of temperatures and salinities near artificially closed boundaries, at the surface, or at depth. The degree of realism of these GCM simulations is unclear.

Existing estimates of the strength and structure of the meridional overturning obtained from different types of studies are not consistent with one another; hydrography-based geostrophic calculations, combination of hydrography with property conservation, and GCM simulations show a large, moderate, and small net northward transport at depth, respectively. Consequently, the corresponding estimates of meridional heat transport differ greatly from one another with a range of 0.25–1.73 PW (1 PW = 10^{15}W). The discrepancies in the estimates of overturning and heat transport pose a great difficulty understanding southern hemisphere thermohaline circulation and heat budget.

Despite efforts to estimate the strength and structure of the overturning of the Indian Ocean, little has been done to investigate the cause of the overturning. On the basis of the results of *Toole and Warren* [1993], *Warren* [1994] used a simple two-layer, two-dimensional (latitude-depth) model to interpret the cause for the meridional overturning. The conclusion is that the net surface heat gain and the differential surface heat flux in the meridional direction drive a vigorous deep overturning. This picture seems to have dominated the perception of the Indian Ocean overturning [see, e.g., *U. S. World Ocean Circulation Experiment*, 1993, p. 5]. However, *Robbins and Toole* [1997] suggest that only one third of their estimated 10 Sv of northward deep inflow upwells to the thermocline. This is inconsistent with *Warren*'s [1994] picture.

The above review highlights the necessity to reexamine the meridional overturning of the Indian Ocean. In particular, studies discussed above indicate that as more data (linear inversions) or more dynamics (GCM simulations) are used, the estimate of the amount of deep water entering the Indian Ocean decreases. Therefore the goal of the present study is to infer the meridional overturning and heat transport of the Indian Ocean by optimally fitting the steady state dynamics of a GCM to climatological data. Specific objectives include the following: (1) to determine whether an optimal solution exists that satisfies the steady state dynamics of a GCM while being consistent with annual mean climatological data within limits of observational uncertainties, (2) to examine whether the meridional overturning derived from the optimal solution is consistent with the conventional picture of a vigorous deep overturning driven by surface buoyancy forcing, (3) to provide an optimal estimate of meridional heat transport and to evaluate its relation to the overturning, and (4) to develop the expertise needed to synthesize the incoming World Ocean Circulation Experiment (WOCE) data into a GCM.

A GCM and its adjoint are used to find a near-steady model trajectory that is consistent with climatological temperatures, salinities, and surface forcings within limits of observational uncertainty. Meridional overturning and heat transport are then determined from such an optimal state. Details of the GCM, the optimization formulation, and the climatological data used are described in section 2. The spinup, i.e., the forward integration of the GCM, is discussed in section 3. In section 4 the meridional overturning and heat transports resulting from several optimization experiments having different imposed constraints are presented, from which we identify a statistically optimal and physically meaningful solution. Section 5 examines the driving mechanism of the meridional overturning, the quality of the optimal solution, the role of sponge layers, and the rectification by seasonal forcings. The findings are summarized in section 6.

This paper focuses on the annual mean meridional overturning and heat transport. All data used to force or constrain the model are climatological annual mean values. There are two major reasons for this effort. First, almost all existing direct estimates from data of the strength of meridional overturning and heat transport of the Indian Ocean are in the context of an assumed annual mean state; the previous interpretation of the driving mechanism of the overturning [*Warren*, 1994] is also in this context. Therefore we want to test whether a climatological annual mean state exists that is consistent with climatological data for the Indian Ocean. If it indeed exists, we evaluate the previous perception in a relevant context. Second, the annual mean inversion establishes a basis to examine the effect of the seasonal cycle. Issues related to the seasonal cycle itself, which is particularly strong in the northern Indian Ocean because of the monsoonal effect, will be addressed in a subsequent paper. However, in this paper we will show that the annual averages derived either from the forward integration of the GCM or from an optimization experiment with seasonal forcings are very similar to those obtained with annual mean forcings. The apparent lack of rectification by the seasonal cycle in the Indian Ocean will be discussed in section 5.4.

Experience with Indian Ocean GCM has been very limited in part due to the open boundaries connecting the Antarctic Circumpolar Current region to the south and connecting the Pacific Ocean to the east via the Indonesian throughflow channel. In particular, there has been no GCM inversion of the Indian Ocean circulation. The only Indian Ocean GCM simulation that explicitly examined the meridional overturning and heat transport [*Wacongne and Pacanowski*, 1996] only used a sponge layer in the southern open boundary and completely closed the Indonesian throughflow channel.

In this study, all open boundaries are formulated as "sponge layers" (closed walls, restoring of temperatures (T) and salinities (S) to prescribed profiles). Although such a boundary treatment cannot model the effect of net mass fluxes into and out of the model domain, baroclinic exchange of mass and fluxes of heat and salt in the vicinity of the boundaries are included. To our knowledge, there has been no attempt to estimate open boundary conditions in a regional GCM (primarily due to the technical complexity). Here we estimate the parameters of the sponge layers as a first step toward open boundary estimation using a GCM and interior climatological data.

2. Model Description

2.1. Data

The climatological annual mean temperatures (T) and salinities (S) used in this study are those provided in the World Ocean Atlas [*Levitus and Boyer*, 1994; *Levitus et al.*, 1994], which were compiled from historical hydrographic data up to 1993. Hereafter, this climatology is referred to as the Levitus

data. The data are mapped to the 1.5°, 24-level model grid from the original 1°, 38-level grid. It is noted that the Levitus data have a several-degree smoothing scale, larger than that of the model horizontal resolution. In situ temperatures are converted to potential temperatures; we will abbreviate potential temperature as T throughout the following discussion.

Table 1 shows the prescribed standard errors of T and S for each model level used to reflect observational uncertainties. These values are chosen in a consistent way using mapping errors of the Levitus data for the Indian Ocean and the errors prescribed by *Marotzke and Wunsch* [1993] for the Atlantic Ocean.

Surface flux data used are annual mean wind stress obtained by *Hellerman and Rosenstein* [1983] and heat and freshwater fluxes provided by *Oberhuber* [1988], all mapped onto the model grid. The assumed errors for these data are 0.5 dyn/cm^2 for wind stress, 50 W/m^2 for heat flux, and 75 mm/yr for freshwater flux.

2.2. GCM and Its Adjoint

The GCM used is the Geophysical Fluid Dynamics Laboratory (GFDL) primitive equation model [*Cox*, 1984]. The horizontal resolution is 1.5° (we have performed test integrations with 1° resolution and the results show little difference). There are 24 vertical levels with the interval between 2 adjacent levels ranging from 25 m near the surface to 500 m near the bottom. The domain is the Indian Ocean north of 32°S with the closed sidewall (Figure 1). A three-point boxcar smoothing both in longitude and in latitude is applied to the raw model topography to obtain a relatively smooth version (the raw topography data are from the "Rand Elevation and Depth Data" [*Gates and Nelson*, 1975] originally compiled at Scripps Institution of Oceanography). Two grid-cell-wide sponge layers, where models T and S are relaxed to some target values, are used near the artificially closed sidewalls that would otherwise be connected to the Antarctic Circumpolar Current to the south, the Indonesian throughflow to the east, and the Red Sea and the Persian Gulf to the northwest. Sponge layers simulate the baroclinic exchange of mass between the model interior and neighboring basins and the input of heat and salt from these basins. Issues related to the net mass flux between the Indian and the Pacific Oceans and between the Indian and the Southern Oceans are left for subsequent effort. Madagascar is flooded with 100 m of water to increase computational efficiency. The adjoint to the GFDL model was originally developed by R. B. Long et al. (Atlantic Oceanographic and Mete-

Table 1. Prescribed Standard Errors of Temperature and Salinity for Various Depths

Depth, m	δ_t, °C	δ_s, psu
12.5	3.08	0.44
37.5	2.93	0.40
62.5	2.61	0.34
87.5	2.07	0.27
125.0	1.53	0.21
200.0	1.20	0.17
300.0	1.13	0.16
400.0	1.11	0.16
500.0	1.07	0.14
600.0	0.96	0.12
700.0	0.84	0.11
850.0	0.70	0.09
1050.0	0.57	0.08
1250.0	0.44	0.07
1500.0	0.32	0.06
1850.0	0.20	0.04
2300.0	0.11	0.02
2800.0	0.06	0.01
3300.0	0.04	0.01
3800.0	0.04	0.01
4300.0	0.04	0.01
4800.0	0.04	0.01
5300.0	0.03	0.01
5800.0	0.01	0.01

Practical salinity unit, psu.

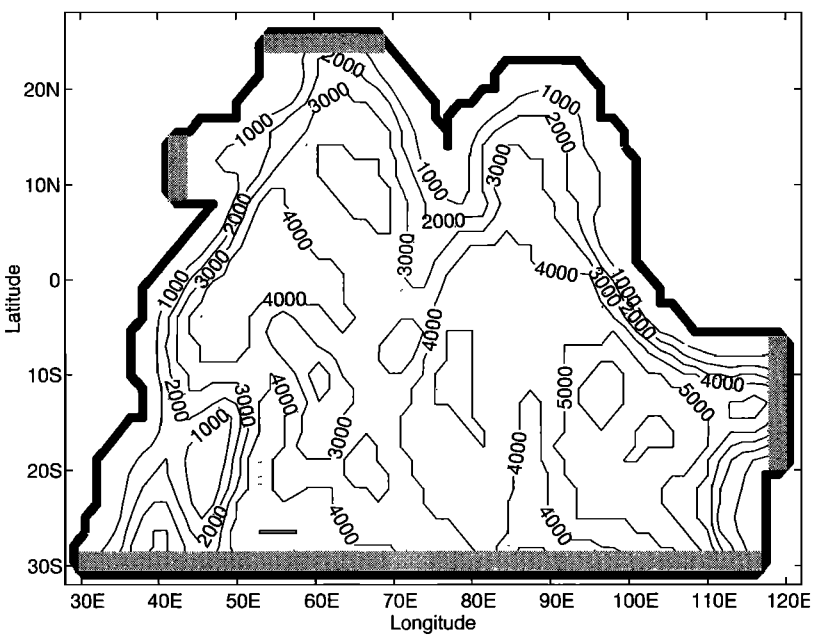

Figure 1. Model geometry and topography. Contours indicate depth in meters. Sponge layers are indicated by shaded areas.

orological Laboratory, unpublished report, 1989) and further implemented by *Tziperman et al.* [1992], *Marotzke* [1992], *Marotzke and Wunsch* [1993], *Bergamasco et al.* [1993], and *Yu and Malanotte-Rizzoli* [1996]. The statistical criteria used to express the constraints to the GCM and the principle of the adjoint method used to enforce the constraints are presented in the following.

A quadratic cost function J is used to penalize the temporal drift of models T and S (the first term) and the model-data misfits of T and S (the second term) in the model interior, the deviations of estimated targets T and S in sponge layers from climatological values (the third term), and the deviations of estimated surface forcings from climatological values (the fourth term)

$$J = \tfrac{1}{2}[(\mathbf{x}_n - \mathbf{x}_0)^T\mathbf{W}_s(\mathbf{x}_n - \mathbf{x}_0) + (\mathbf{x}_n - \mathbf{x}_d)^T\mathbf{W}_d(\mathbf{x}_n - \mathbf{x}_d) + (\mathbf{x}^s - \mathbf{x}^s_d)^T\mathbf{W}^s_d(\mathbf{x}^s - \mathbf{x}^s_d) + (\mathbf{f} - \mathbf{f}_d)^T\mathbf{W}_f(\mathbf{f} - \mathbf{f}_d)],$$

where $\mathbf{x}_0$ and $\mathbf{x}_n$ are vectors of model variables (T and S) at the beginning and the end of the forward integration and $\mathbf{x}_d$ is the observed T and S. The subscripts s and d stand for steadiness and data, whereas the superscript s stands for sponge layer. The elements of these vectors correspond to different grid points. The estimated and observed surface forcings are $\mathbf{f}$ and $\mathbf{f}_d$; $\mathbf{W}_d$ and $\mathbf{W}_f$ are weight matrices for the model-data misfits of T and S and surface forcings, which ideally would be the inverse observational error covariance matrices. Each diagonal element in these matrices is the variance of data errors at a grid point. By assuming independent data errors at different grid points, the off-diagonal elements (the spatial covariances) are set to zero. $\mathbf{W}_s$ is a weighting matrix for the temporal drift. The ratio of $\mathbf{W}_s$ and $\mathbf{W}_d$ reflects how strongly the steadiness constraint is enforced, which depends on the total integration period of the model. Following *Marotzke* [1992], we demand that the temporal drift of the model in an effective 10-year integration period should be equivalent to observational uncertainties. Since the actual integration time is one year, $\mathbf{W}_s$ is set to $10^{-2} \times \mathbf{W}_d$. In other words, the temporal drift of T and S for the 1-year integration period should be equivalent to one-tenth of the observational errors. Velocities, which are not constrained in the present study, adjust to the optimal estimates of T and S. The third term in J marks a major difference from the conventional sponge layer treatment in regional GCM where the models T and S are simply relaxed toward fixed targets T and S either taken from climatology or a hydrographic section. The merit of this optimal treatment of sponge layer will be illustrated by experiments with and without the sponge layer estimation.

The cost function J is minimized by optimally adjusting the control variables, which are the initial state (T and S), side boundary properties (targets T and S in sponge layers), and surface forcings, subject to the constraints that model dynamics are fulfilled. In other words, optimal sets of initial and boundary conditions are sought. This constrained minimization problem is transformed into an unconstrained one by introducing an extended cost function $L = J + \lambda F(\mathbf{x}, \mathbf{f})$, where λ is called "Lagrange multiplier" and $F(\mathbf{x}, \mathbf{f}) = 0$ is the dynamical model equation. Setting $\partial L/\partial\lambda = 0$ gives the model equation, called the forward model here. Setting $\partial L/\partial\mathbf{x} = 0$ gives the adjoint to the forward model. Integration of the forward model results in a certain temporal drift and model-data misfit. The adjoint, forced by the temporal drift and model-data misfit, integrates backward in time calculating λ as solution. After integrating back to the initial time, it provides the gradients of L with respect to the control variables (initial conditions, side boundary properties, and surface forcings $\mathbf{x}_0$, $\mathbf{x}^s$, $\mathbf{f}$: $\partial L/\partial\mathbf{x}_0$, $\partial L/\partial\mathbf{x}^s$, and $\partial/\partial\mathbf{f}$). A conjugate gradient descent algorithm uses these gradients to determine the "downhill" direction of L and the optimal magnitude of correction of $\mathbf{x}_0$, $\mathbf{x}^s$, and $\mathbf{f}$ along that direction. The procedure is then repeated until a minimum of J is found. In practice, the iterative procedure is stopped when it does not bring about a significant reduction in cost or when the total cost is below a statistically acceptable level (the misfit is smaller than the prescribed data error). Detailed descriptions of the adjoint formulation can be found in works by *Thacker and Long* [1988], *Sheinbaum and Anderson* [1990], *Smedstad and O'Brien* [1991], and *Marotzke and Wunsch* [1993].

3. Spinup

Before discussing the optimization experiments, we first present results of the spinup, i.e., a forward integration of the GCM. This serves two purposes: (1) the product of the spinup is a natural choice of a dynamically balanced field to initialize the optimization runs and (2) the result of the spinup provides a comparison with optimized solutions presented later on.

In the spinup the model is initialized from annual mean climatological T and S and forced at the surface by climatological wind stress as well as heat and freshwater fluxes in combination with a relaxation toward climatological sea surface temperatures (SSTs) and salinities using a timescale of 1 day. This relaxation timescale is much shorter than the ones used conventionally (1–2 months or even longer) because model SST at the equilibrium state is several degrees higher than climatological values if a timescale as long as 1 month is used. The targets T and S in all sponges are set to climatological values. The relaxation times are 1 and 5 days for the outer and inner grids, respectively.

The model reaches a near-equilibrium state after 100 years of integration. The resultant meridional overturning stream function (i.e., zonally integrated meridional velocity integrated from the surface) is shown in Figure 2a. It is dominated by a clockwise overturning cell roughly between 300 and 3000 m with a strength of 22 Sv. Above this dominant cell there is a shallow overturning of opposite direction with a strength of 12 Sv. The dominant overturning cell with interior downwelling and deep outflow is contrary to the conventional picture of the overturning of the Indian Ocean. Following the experience of *Döscher et al.* [1994] in the simulation of the North Atlantic circulation, we integrated the model by replacing the climatological targets T and S in the southern sponge with those directly mapped from the 32°S section analyzed by *Toole and Warren* [1993]; the resultant stream function remains similar, however. This is because the 32°S section comprises most of the data at nearby latitudes in the *Levitus and Boyer* [1994] and *Levitus et al.* [1994] climatology. We have also used the version of *Levitus* [1982] climatology (in which the Toole and Warren section was not included) as sponge layer targets T and S; the resulting stream function is similar, but the magnitude of the reverse overturning becomes weaker by several Sv.

Lack of seasonal forcings are not responsible for the reverse overturning because the annual average overturning from the forward integration with seasonal surface and side boundary forcings (Figure 2b) is very close to that with annual mean forcings. We will return to the apparent lack of seasonal rec-

tification of the model Indian Ocean later on. The reverse overturning resulting from our forward integration is similar to that in the seasonally forced run by *Wacongne and Pacanowski* [1996]. However, the magnitude of their reverse overturning is smaller, probably due to the use of a longer relaxation time (toward the Levitus data) in their thick sponge layer which extends from about 15° to 32°S. We believe that the cause for the reverse overturning in that study is the same as that here: the biased zonal gradients of targets T and S that were mapped to the model grid either from the Levitus data or from a hydrographic section. This will be discussed in detail in sections 4.1 and 5.3.

The final state of the 1-year spinup (by which time a dynamically balanced state has been achieved) is used to initialize the optimization experiments. The 100-year integration is not used because the model state after such a long integration drifted relatively far away from climatological T and S. Notice that the equilibrium time of the integration is surprisingly short and probably governed by wave dynamics. The details of the adjustment are beyond the scope of this paper and will be presented elsewhere.

4. Optimization Experiments

In this section we present results of four optimization experiments to investigate the strength and structure of the meridional overturning as well as the heat transport and its relation to the overturning. The data and steadiness constraints as well as surface forcing penalty imposed on the GCM, as shown by the first, second, and fourth terms of the cost function J (see section 2), are the same for all experiments. Likewise, optimal initial conditions for T and S, wind stress, as well as surface heat and freshwater fluxes are estimated in all experiments. However, the treatment of boundary condition in the sponges is different. Run A keeps targets T and S in sponges fixed, while run B treats them as control variables and provides new estimates. In other words, the third term in J is enforced in run B but not in run A. Run C is like run B, but an additional constraint is imposed on the zonally integrated transport from the southern sponge into the interior below 2000 m. Run D is similar to run C except that the targets T and S in the throughflow sponge are fixed (for reasons that will become clear). The timescales at which models T and S are relaxed toward target values in sponges are the same in all experiments. For all experiments the end products at the 80th iteration will be discussed, at which the total cost function has been reduced to a statistically acceptable level and the optimization would not bring about significant change.

4.1. Meridional Overturning

Run A. In this experiment, the targets T and S in sponge layers are fixed to climatological values just as the spinup. The value of the total cost for T and S as a function of iteration (dashed-dotted curve in Figure 3) indicates that both the steadiness and data costs have been reduced to an overall acceptable level (a data cost of unity means that, overall, model-data misfit is smaller than the prescribed data error). Although the model state is now closer to the Levitus data than the spinup, the meridional stream function (Figure 4a) is similar to the one resulting from the spinup.

As the stream function shows, the net northward flow above the zero stream line (above 300 m or so) upwells to the surface to balance the net southward flow near the surface. The portion of net northward flow below 300 m eventually downwells and returns to the south below 1250 m. This is because the total transport of northward flow exceeds that of the near-surface southward flow. Because of the continuity requirement the excess northward flow has to downwell and return to the south at depth rather than upwell to the surface.

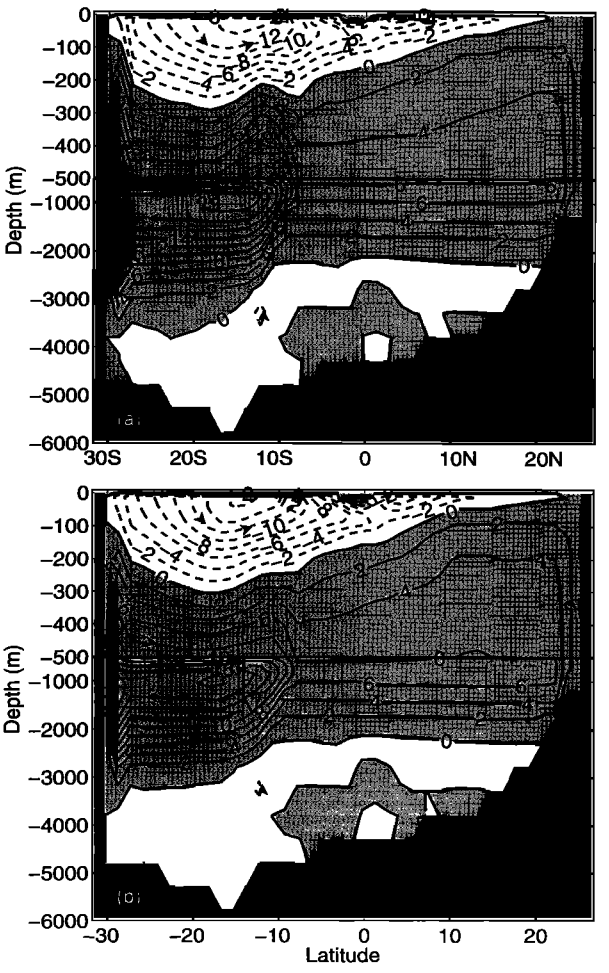

Figure 2. (a) Meridional stream function resulting from 100 years of forward integration with constant annual mean (surface and side boundary) forcings. (b) The annual average stream function with seasonal forcings (contour interval is 2 Sv).

The cause for the excess net northward flow is that the total southward transport carried by western boundary currents, the Agulhas and East Madagascar Currents, is too small. First, waters from the southern sponge is going into the Mozambique Channel above ~1500 m and west of 42°E, and the Agulhas Current has a wrong direction, as shown by the meridional velocity at the edge of the southern sponge (Figure 4b) and horizontal velocities at the 500-m depth (Figure 5b). Second, it is not obvious from this experiment alone that the East Madagascar Current is too weak, but this will become clear when a comparison with subsequent experiments is undertaken later.

Flows across the edge of the southern sponge are basically determined by the zonal density gradient along the edge of the sponge through the geostrophic balance. Thus the zonal density structure in the sponge (especially that near the Agulhas and East Madagascar Currents), fixed to the Levitus data in this run, is responsible for the unrealistic transports of Agulhas and East Madagascar Currents. Interior data constraints are

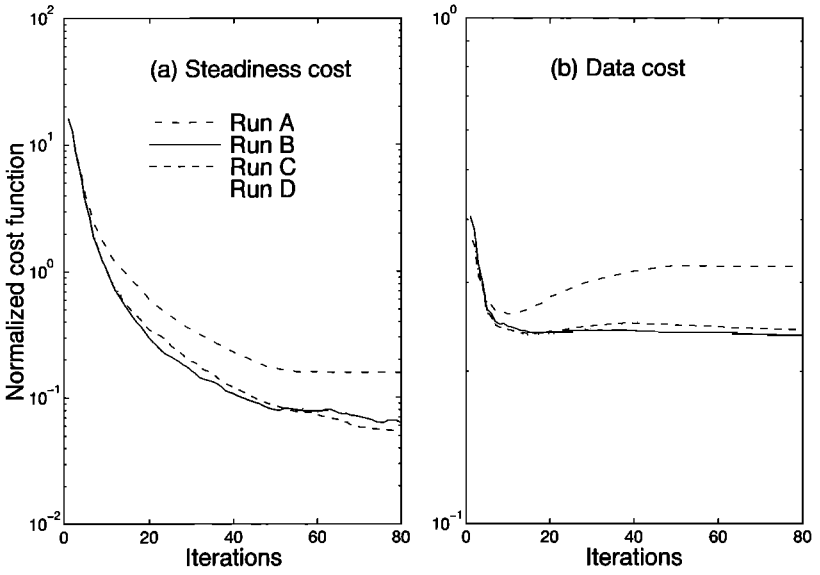

Figure 3. Normalized (a) temporal drift and (b) model-data misfit.

too weak to compete with the strong constraint in the sponge. There are several possible causes for the undesirable zonal target temperature gradient such as eddy signal in hydrographic data, mapping error, etc.

Horizontal circulation associated with the overturning, together with temperature changes across the southern and throughflow sponges, results in systematic warming and cooling patterns with time at different depths of the model interior.

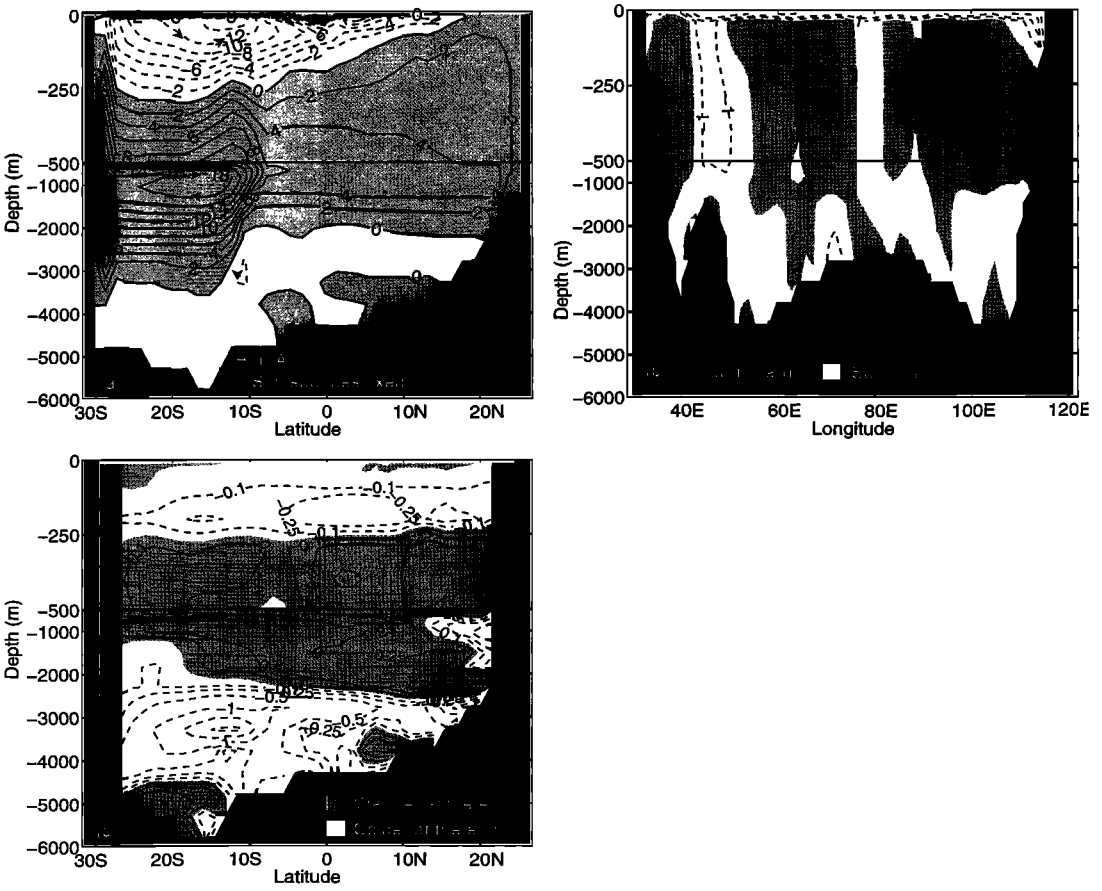

Figure 4. (a) Meridional stream function, (b) meridional velocity section at the edge of the southern sponge, and (c) normalized temporal drift of zonally averaged temperature for run A. Contour interval in Figure 4a is 2 Sv; contour levels in Figure 4b are −8, −4, −2, −1, 1, 2, 4, and 8 cm/s. Southern and northern sponge layers are masked out in Figure 4c. In Figures 4a–c, shaded areas indicate positive values.

Temporal drift of salinity will not be discussed because temperature effects dominate. As illustrated by Figure 5b, the northward flowing waters are largely carried by the current in the Mozambique Channel, which joins the model Somali Current farther north. Some of these waters travel to the northern Indian Ocean where they downwell. Since the target temperatures in the southern sponge between 400 and 1200 m are higher than interior temperatures (not shown), these excess northward flowing warm waters and downwelling cause a warming pattern in the interior for about the same depth range (Figure 4c). Some of the northward flowing waters turn eastward and enter the throughflow sponge above 1300 m (Figure 5b), where they downwell and return to the interior and spread both to the south and the north (Figure 5c). Since these waters acquire target temperatures of the throughflow sponge that are lower than interior temperatures, they result in a cooling pattern below 1300 m (Figure 4c). The vertical profile of meridionally averaged zonal velocity at the edge of the throughflow sponge (thin solid curve in Figure 6) implies an unrealistically large baroclinic exchange of mass near the throughflow region. Up to 15 Sv come out of the throughflow sponge below 1300, quite inconsistent with geostrophic calculations and limited current meter measurements which suggest that the Indonesian throughflow is confined to the top 200 m or so [*Fieux et al.*, 1994; *Meyers et al.*, 1995].

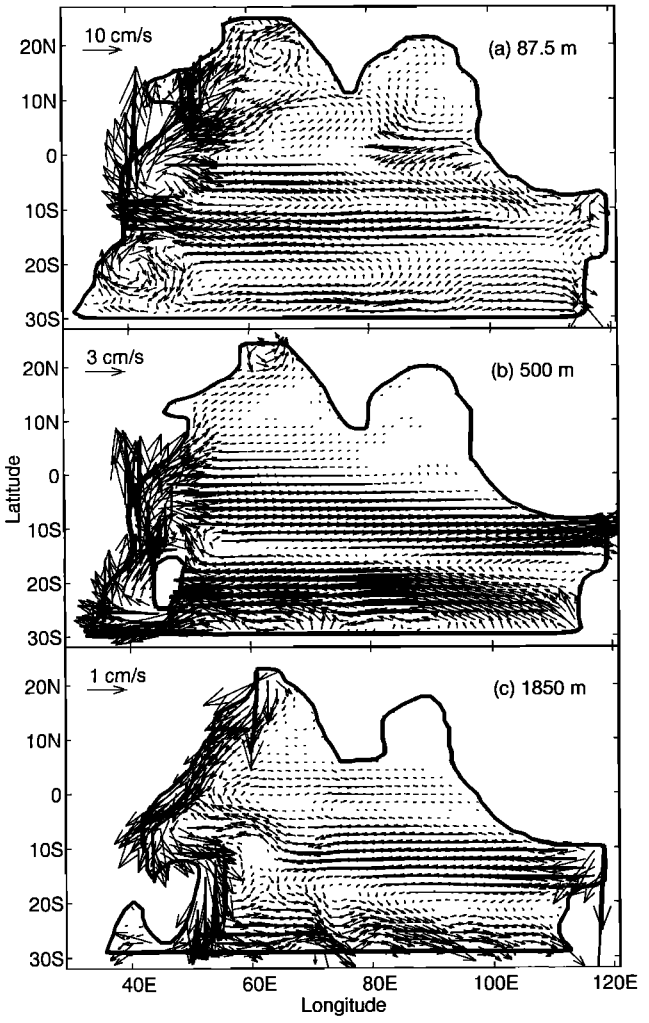

Figure 5. Horizontal velocities of run A at (a) 87.5, (b) 500, and (c) 1850 m.

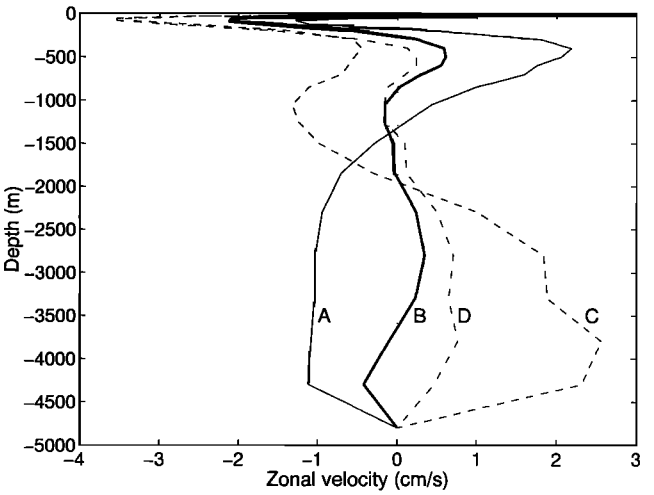

Figure 6. Meridionally averaged zonal velocity at the edge of the throughflow sponge for the four experiments.

Run B. Run A indicates that target temperatures in the southern sponge play a key role in determining the meridional overturning as well as the horizontal circulation. Data constraints in the model interior surrender to the fixed zonal gradients of target temperatures which set the baroclinic mass exchange between the sponge and the interior. In order to cure this problem, targets T and S in all sponges are treated as control variables in this experiment and estimated as part of the optimization procedure. In other words, the third term of the cost function J is enforced to penalize deviations of estimated targets T and S from climatological values with very small weights. Targets T and S, initialized by climatological values, are adjusted during the optimization procedure so as to reduce the total cost and biased residual patterns such as the temporal drifts seen in run A.

The resultant overturning (Figure 7a) is now dominated by a shallow (<1000 m) overturning cell having a strength of about 14 Sv with southward flowing near-surface waters and northward flowing thermocline waters. The overturning at depth is very weak with only 2 Sv of net northward transport below 1000 m. The reverse overturning as seen in run A disappears primarily because of the strengthened southward transport from the interior to the southern sponge associated with the two Western Boundary Currents: the southward flowing Agulhas Current is now present, and the East Madagascar Current becomes stronger, as shown by the meridional velocity section near the southern sponge (Figure 7b) and the horizontal velocities at various depths (Figure 8). These changes are results of the optimal adjustment of target temperatures. The zonal section of target temperatures at the edge of the southern sponge (Figure 9) indicates that near the Agulhas and East Madagascar Currents (~35° and 50°E) the zonal temperature gradients, $\partial T/\partial x$, are more positive (upward tilt of isotherms toward the west) in run B (solid contours) than they are in run A (dashed contours). The corresponding change in vertical shear achieved through the thermal wind relation results in the southward flowing Agulhas Current and a stronger East Madagascar Current.

The 2 Sv or so of net northward transport at depth is due to the difference between several bands of northward flows and

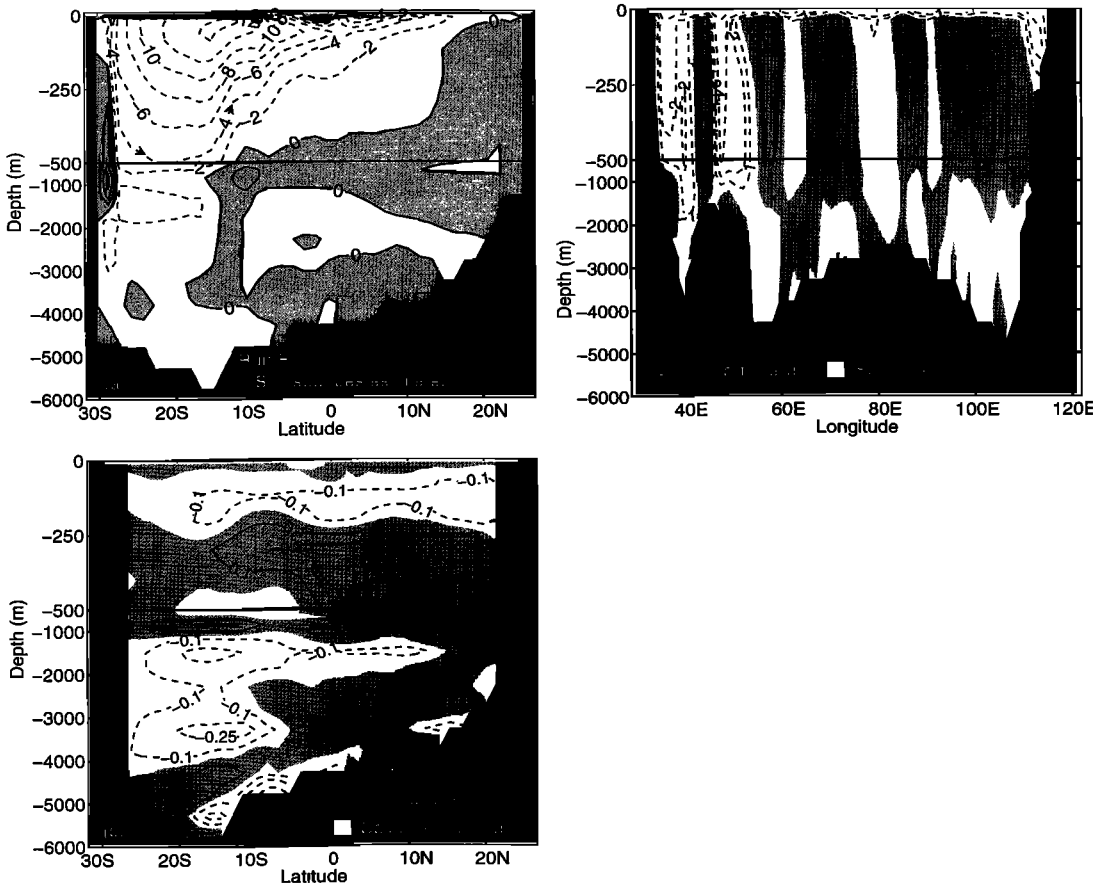

Figure 7. (a) Meridional stream function, (b) meridional velocity section at the edge of the southern sponge, and (c) normalized temporal drift of zonally averaged temperature for run B. Contour interval in Figure 7a is 2 Sv; contour levels in Figure 7b are −8, −4, −2, −1, 1, 2, 4, and 8 cm/s. Southern and northern sponge layers are masked out in Figure 7c. In Figures 7a–c, shaded areas indicate positive values.

the southward recirculations. The meridional velocity section (Figure 7b) shows a well-established DWBC pressing against the Madagascar Ridge near 48°E; there is also a weak signature of DWBCs near the Central Indian Ridge near 78°E and near the Ninetyeast Ridge.

The optimal treatment of targets T and S leads to a steadier solution that is closer to climatological data, as shown by the total steadiness and data cost (solid curve in Figure 3). The steadiness residuals of zonally averaged temperatures now show little temporal drifts (Figure 7c). The warming pattern seen in run A (Figure 4c) disappears because there is no excess northward flowing warm waters and interior downwelling. Consequently, there is little baroclinic exchange across the throughflow sponge at depth (thick solid curve in Figure 6). Thus the cooling trend at depth found in run A is eliminated.

Run C. Although estimation of targets T and S in sponges in run B greatly improves the estimated state of the Indian Ocean both statistically and physically, the amount of deep water entering the interior from the southern sponge, 2 Sv below 2000 m, is much smaller than the 27 Sv suggested by *Toole and Warren* [1993]. To examine whether the model can accommodate a large net northward transport at depth with some extra constraints, in this experiment we require 27 ± 27 Sv of zonally averaged northward flow from the southern sponge into the interior below 2000 m. All other constraints are the same as those of run B. The cost function now becomes

$$J = \tfrac{1}{2}[(\mathbf{x}_n - \mathbf{x}_0)^T\mathbf{W}_s(\mathbf{x}_n - \mathbf{x}_0) + (\mathbf{x}_n - \mathbf{x}_d)^T\mathbf{W}_d(\mathbf{x}_n - \mathbf{x}_d) + (\mathbf{x}^s - \mathbf{x}_d^s)^T\mathbf{W}_d^s(\mathbf{x}^s - \mathbf{x}_d^s) + (\mathbf{f} - \mathbf{f}_d)^T\mathbf{W}_f(\mathbf{f} - \mathbf{f}_d)] + \frac{1}{2}\left(\frac{1}{27}\right)^2 (V - 27)^2,$$

where $V = \int_{\text{bottom}}^{2000}\int_{x_w}^{x_e} v dx dz$ is the total northward transport (in Sv) below 2000 m from the southern sponge into the model interior (v is the meridional velocity at the edge of the southern sponge). Note that the penalty for the deviation of net northward transport below 2000 m from 27 Sv is the same as that for the deviations of T and S from climatological values integrated over all grid points.

The strength of the resultant overturning (Figure 10a) above the 1000-m level is slightly larger than that of run B (16 Sv versus 14 Sv of run B). This is associated with stronger Agulhas and East Madagascar Currents, shown in meridional velocities at the edge of the southern sponge (Figure 10b), set by zonal gradients of estimated target temperatures in the southern sponge. Note that the banded feature of meridional velocities shown in Figure 10b is due to vertically coherent horizontal vortices generated by large vertical velocities in the sponge as discussed by *Klinck* [1995]. The overturning around 2000 m achieves a strength of 21 Sv due to the deep inflow requirement. Although the model can now accommodate a large net

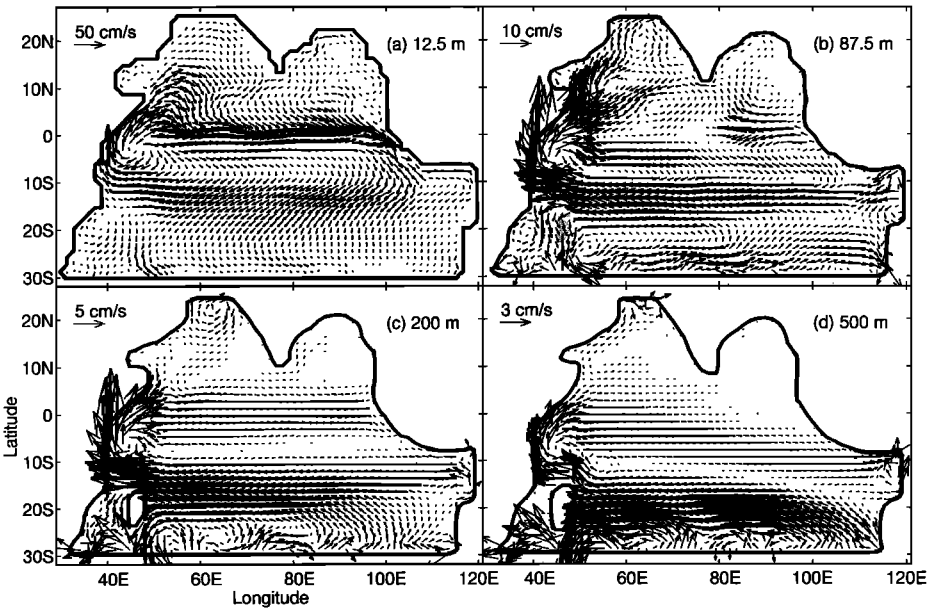

Figure 8. Horizontal velocities of run B at (a) 12.5, (b) 87.5, (c) 200, and (d) 500 m.

northward transport at depth, the northward flowing waters do not upwell in the interior as indicated by the near-horizontal orientation of the streamlines below 2000 m. Instead, they move northward and turn into the throughflow sponge below 2000 m (Figure 11c). The model provides strong heating in this sponge by raising target temperatures to convert the incoming cold waters into warmer waters at shallower levels (<2000 m) where they come back into the interior; some of them find their way back to the southern sponge, while others travel across the basin to join the current in the Mozambique Channel and East Madagascar Current (Figures 11a and 11b), which explains why the two currents in this run are stronger than they were in run B.

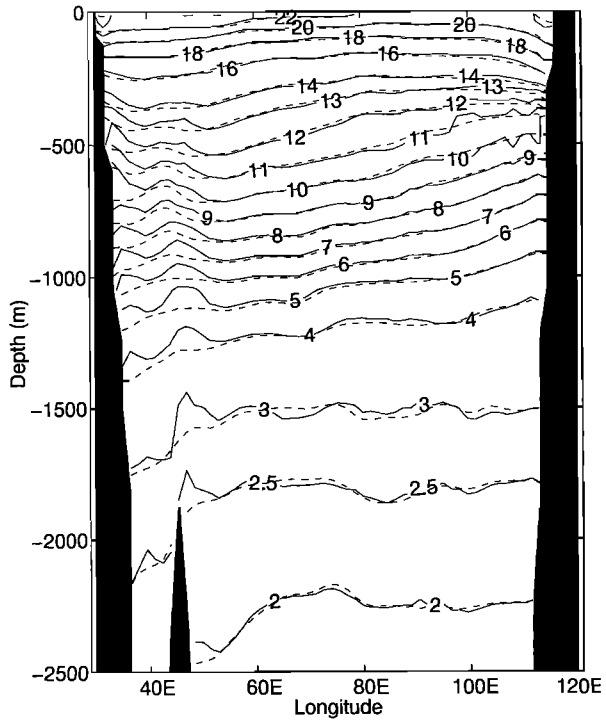

Figure 9. Zonal section of target temperatures at the edge of the southern sponge. Run A, dashed contours; run B, solid contours.

The strong upwelling inside the throughflow sponge gives rise to the abrupt rise of streamlines between 13° and 11°S in the stream function plot. The steadiness residual of temperatures (Figure 10c) shows a cooling trend below 2000 m and south of 10°S indicating that the large volume of cold waters required to come out of the southern sponge is in conflict with the steady state dynamics of the model. The cooling trend is absent north of the throughflow latitudes because the cold water masses were destroyed in that sponge by large heating.

The requirement of large net northward transport below 2000 m results in 21 Sv of waters flowing in and out of the throughflow sponge separated by the 2000-m level (dashed curve in Figure 6). This is too large to be consistent with existing analysis of hydrography [*Fieux et al.*, 1994; *Meyers et al.*, 1995]. Around the 2000-m level which delimits flows in and out of the throughflow sponge, horizontal advection and diffusion of heat are not very important; upward advection of cold waters is thus primarily balanced by artificial heat input through the relaxation. This artificial heating can be interpreted as an effective vertical mixing; assuming a balance between vertical advection and effective diffusion around the 2000-m level, $\kappa_T(\partial^2 T/\partial z^2) = w(\partial T/\partial z)$, the resultant effective diffusivity κ_T is about 1000–2000 cm^2/s, which is implausible.

Statistically speaking, runs B and C are not much different because the total temporal drifts and model-data misfits of these two runs (solid curve and dashed curve in Figure 3) are close. It is the large baroclinic mass exchange and the implied magnitude of vertical mixing in the throughflow sponge that render run C physically unrealistic. Therefore, when fitting dynamics to data, one should not only focus on residual statistics but also examine the physical soundness of the solution.

Run D. From run C it is seen that target temperatures in the throughflow sponge are raised to provide strong heating to

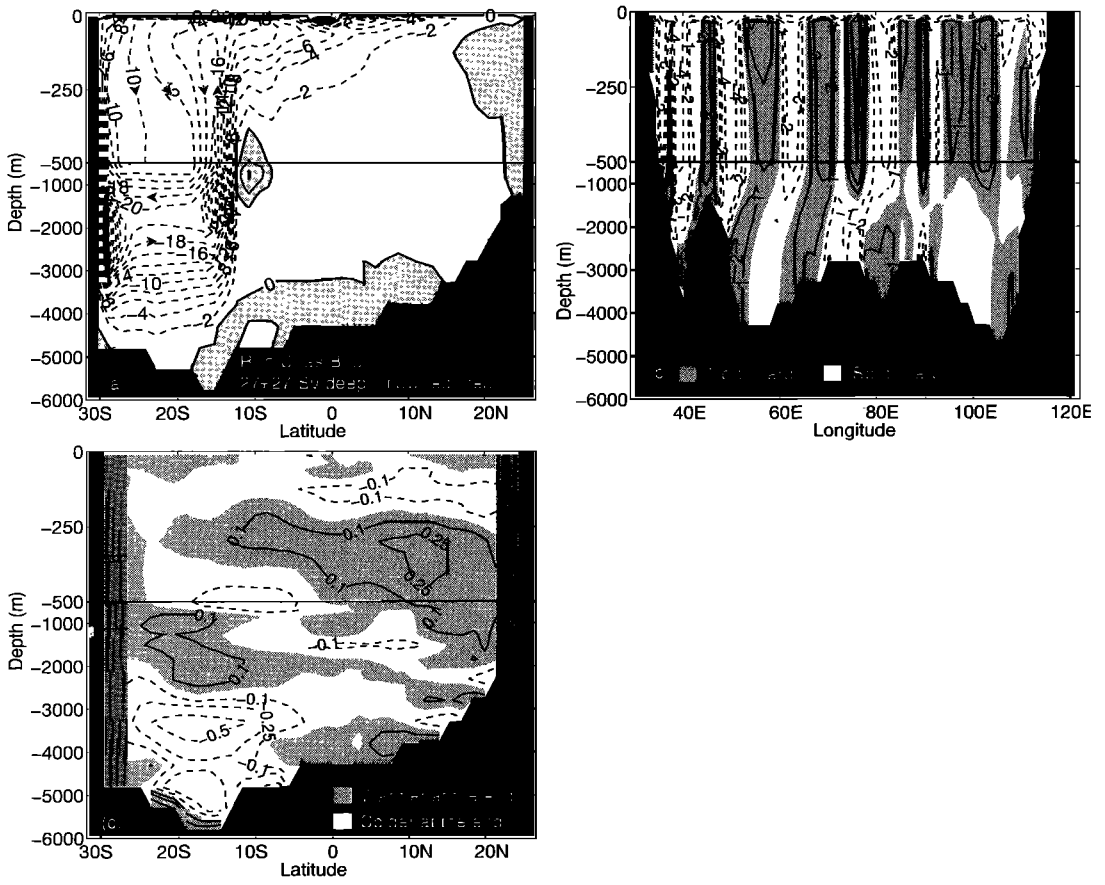

Figure 10. (a) Meridional stream function, (b) meridional velocity section at the edge of the southern sponge, and (c) normalized temporal drift of zonally averaged temperature for run C. Contour interval in Figure 10a is 2 Sv; contour levels in Figure 10b are −8, −4, −2, −1, 1, 2, 4, and 8 cm/s. Southern and northern sponge layers are masked out in Figure 10c. In Figures 10a–10c, shaded areas indicate positive values.

destroy the large net northward transport of cold waters from the southern sponge. To examine the sensitivity of the overturning strength to target temperatures in the throughflow sponge in run D, we keep all constraints the same as those of run C except that targets T and S in the throughflow sponge are fixed to climatology.

The resultant overturning (Figure 12a) in the upper 1000 m is similar to that of runs B and C and has a strength of 15 Sv, in between those of runs B and C. At depth the model can only accommodate about 10 Sv of northward flow below 2000 m. Approximately 2 Sv (e.g., the 10 Sv streamline) of the deep flow upwell in the interior and return to the south at the depth of 1500 m. The other 8 Sv of water behave similar to the deep flows of run C; they travel horizontally to the north, and a large portion of them (7 Sv) turn into the throughflow sponge where they upwell and return to the interior (dotted-dashed curve in Figure 6) in a way similar to that of run C. The reason that this run supports less northward transport at depth is because target temperatures in the throughflow sponge are fixed to climatological values and so are unable to provide as strong a heating as that of run C. Although the baroclinic mass exchange near the throughflow region is much reduced as compared with that of run D (7 versus 21 Sv), it still implies a very large vertical diffusivity of temperature (about 500 cm^2/s) based on the advective-diffusive balance in the vertical.

The steadiness residuals (Figure 12c) show a large cooling pattern below 2000 m, which extends much farther to the north than that of run C (Figure 10c). This, again, is an indication that large northward transport is inconsistent with steady state dynamics of the model. In fact, model temperatures between the southern and throughflow sponge at depths below 2000 m are now systematically colder than climatological values (not shown).

Therefore estimating targets T and S in the throughflow sponge causes a significant change in the strength of the overturning if a large northward transport at depth is required. This, however, is not true without this requirement; an experiment similar to run B but with fixed targets T and S in the throughflow sponge results in a solution that is very similar to that of run B.

4.2. Meridional Velocities

On the basis of the discussion in section 4.1 it is concluded that run B is the best solution of all four experiments because its circulation is the most realistic and the total final cost the smallest, which is largely due to the smaller data cost (Figure 3b). However, residual statistics is not as strong an argument as the physical realism because in comparing the residuals one should take into account the difference in the number of degrees of freedom for different experiments. In the following, the zonal structure associated with the dominant overturning is discussed focusing on run B, the optimal solution.

The zonal structure of mass balance associated with the meridional overturning is latitude dependent. Zonal sections of meridional velocities of run B at several representative latitudes are shown in Figure 13. From the southern boundary to about 10°S the broad northward interior flows below the surface level and above 1000 m are balanced by the southward flowing Agulhas Current (or the flow through the Mozambique Channel) and East Madagascar Current in the western part of the basin, the Leeuwin Current along the west coast of Australia, and Ekman flow at the surface layer (Figure 13a). Between 10°S and the equator the northward component of the Somali Current is balanced by southward Ekman and weak interior flows (Figure 13b). Near the equator (Figure 13c) the balance is more complicated because of the presence of zonal jets which reverse direction with depth. In the upper 500 m apart from the Somali Current which crosses the equator near the western boundary, there are several 100-m-thick layers of opposite-flowing waters spanning almost over the whole basin. It is uncertain whether these layers are related to actual cross-equatorial exchanges or just model artifacts. The picture north of the equator is even more complex. Overall we conclude that there is no simple three-dimensional transport structure that explains the zonally integrated overturning.

4.3. Meridional Heat Transport

For all experiments the meridional heat transport is close to the total advective heat transport; diffusion plays an insignificant role. The total advective heat transport can be decomposed into two components, one resulting from the vertical correlation of zonally averaged temperature and meridional velocity (the "overturning contribution") and one from the correlation between deviations from the zonal averages (the "gyre contribution"). An example is illustrated in Figure 14 (run B). The overturning has a much larger contribution to heat transport than does the horizontal gyre. One could further decompose the overturning contribution into two parts: the portion due to near-surface Ekman transport and the subsurface compensating flow, and the remaining portion that is associated with thermohaline overturning. The two components reflect the relative importance of wind and surface buoyancy forcings in terms of heat transport. We will not present such a partition because of the lack of a satisfactory criterion to define the vertical structure of Ekman and compensating flows.

The climatological surface heat flux integrated from the northern boundary to various latitudes is shown in Figure 15 (thin dashed curve). The same for the estimated surface heat flux of run B is indicated by the thin solid curve in Figure 15. Those of runs A, C, and D are similar and thus not shown. The integrated estimates of surface heat flux are consistently smaller in magnitude than the integrated climatological heat flux north of 15°S (which roughly corresponds to the line where heat gain changes to heat loss).

In equilibrium, surface heat gain must be balanced by southward heat transport. The total southward heat transports of the four experiments are also shown in Figure 15. That of run A (dotted curve) is unrealistic because it is much smaller in magnitude than the heat transport implied by the estimated surface heat flux (the thin solid curve). This is because the only major contributor to southward heat transport for this run is a shallow overturning cell above 300 m. The 2 Sv or so overturning below 3000 m transport very little heat to the south. The dominant overturning between 300 and 3000 m results in northward heat transport. Consequently, the total heat transport is southward only between 12°S and 7°N where southward heat transport due to the upper cell exceeds the northward heat transport associated with the dominant cell at middle depth. The insufficient southward transport also explains the systematic warming trend of model state of this run.

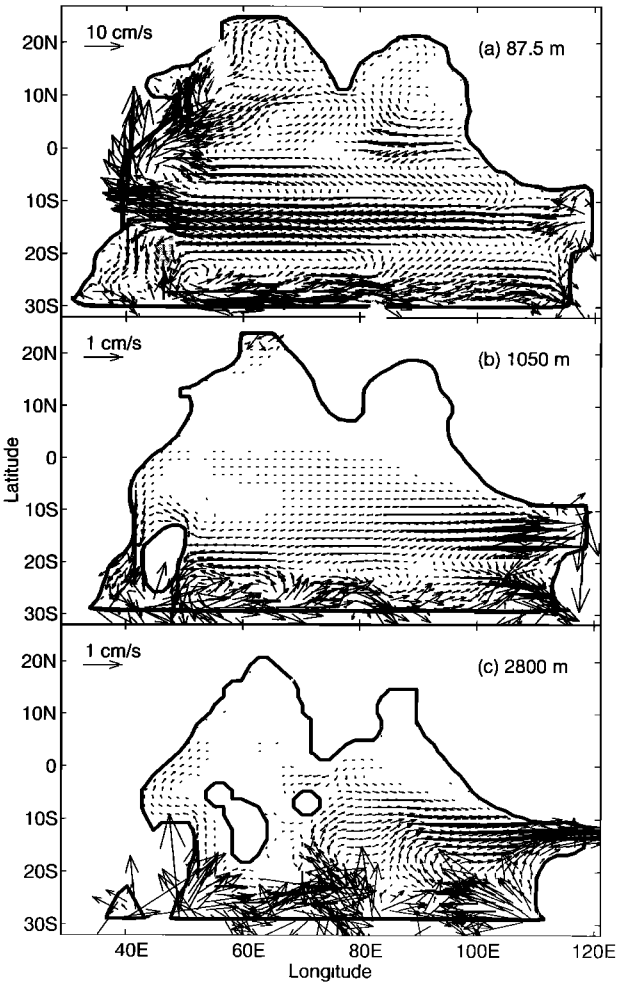

Figure 11. Horizontal velocities of run C at (a) 87.5, (b) 1050, and (c) 2800 m.

For run B the heat transport in Figure 15 (thick solid curve) is southward almost everywhere with a maximum of 0.83 PW near 15°W. It is much closer to the integrated heat flux estimate than run A. This implies that the meridional overturning of run B serves to compensate the estimated surface heat gain. Again, the shallow overturning cell in the upper 1000 m is the major contributor to the model heat transport; the weak overturning at depth has little contribution. If there is no heat flux through any side boundary, the model heat transport should coincide with the integrated surface heat flux estimate. However, there is a net outward heat flux across the Persian Gulf sponge (warmer water enters and colder water leaves the sponge) and a net inward heat flux across the throughflow sponge. These heat sink and source result in offsets between model heat transport and the integrated heat flux estimate. The southward heat transport at 18°S, 0.79 PW, is somewhat larger than *Fu*'s [1986] estimate of 0.69 PW at the same latitude, but smaller than *Macdonald*'s [1995] estimate of 1.45 PW based on regional and global linear inversions of hydrographic section data. The heat transport near the model southern

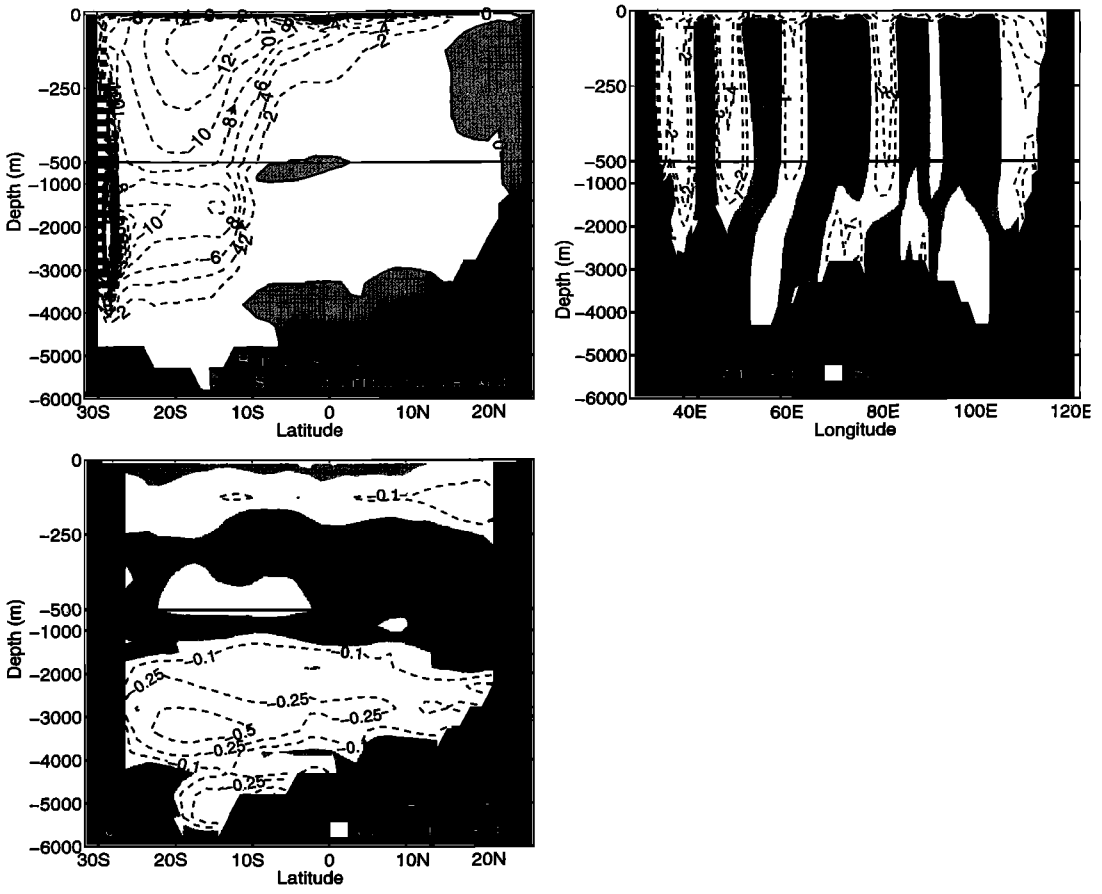

Figure 12. (a) Meridional stream function, (b) meridional velocity section at the edge of the southern sponge, and (c) normalized temporal drift of zonally averaged temperature for run D. Contour interval in Figure 12a is 2 Sv; contour levels in Figure 12b are −8, −4, −2, −1, 1, 2, 4, and 8 cm/s. Southern and northern sponge layers are masked out in Figure 12c. In Figures 12a–12c, shaded areas indicate positive values.

boundary, about 0.5 PW, is again larger than Fu's estimate of 0.25 PW and smaller than Macdonald's estimate of 1.3 PW, both at 32°S. The southward heat transports of the present study are larger than those estimated by *McCreary et al.* [1993] (using a 2½-layer model for a similar horizontal domain) by about 70%.

The heat transport of run C in Figure 15 (thick dashed curve) is close to that of run B north of the throughflow latitudes (13°–11°S). Near and south of the throughflow region, however, the southward heat transport is well over what is needed for the compensation of the net surface heat gain. This excess amount of model heat transport is due to the conversion of the 21 Sv of northward flowing cold waters below 2000 m into southward flowing warmer waters above that level in the throughflow sponge. Therefore this portion of the heat transport has no relation to the surface heat gain. The heat transport of run D in Figure 15 (thick dashed-dotted curve) is similar to that of run C except that the southward excess heat transport is smaller in magnitude because the overturning at depth is weaker.

We conclude that modeled surface thermal forcing does not necessary demand a vigorous deep overturning and that the net surface heat gain can be compensated by shallow overturning, in contrast with the previous perception that surface buoyancy forcing drives a deep meridional overturning of the Indian Ocean [*Warren*, 1994].

The systematically smaller estimated surface heat gain compared to climatology has two possible causes: (1) the climatological heat flux overestimates the actual heat gain by the Indian Ocean and (2) the model has difficulty transporting the actual amount of surface heat gain to the south. We are unable to distinguish between the two from our results.

5. Discussion

5.1. Buoyancy Versus Wind Forcings

Although the net surface heat gain is compensated by southward heat transport associated with a shallow overturning in run B, it is not necessarily true that the shallow overturning is caused by buoyancy forcing. The overturning enclosed by the negative 6-Sv streamline in the southern Indian Ocean appears to be a secondary circulation of the subtropical front between 10° and 20°S in the upper few hundred meters (Figure 8). This front is wind driven and closely resembles the wind stress pattern for that latitude band. The equatorial jet at the first level, which is also wind driven, is associated with two shallow secondary circulations on both side of the equator with opposite signs.

To test the relative importance of wind and buoyancy forcings to meridional overturning and heat transport, we perform two forward integrations using the end product of run B as initialization. In the first one, surface heat and freshwater

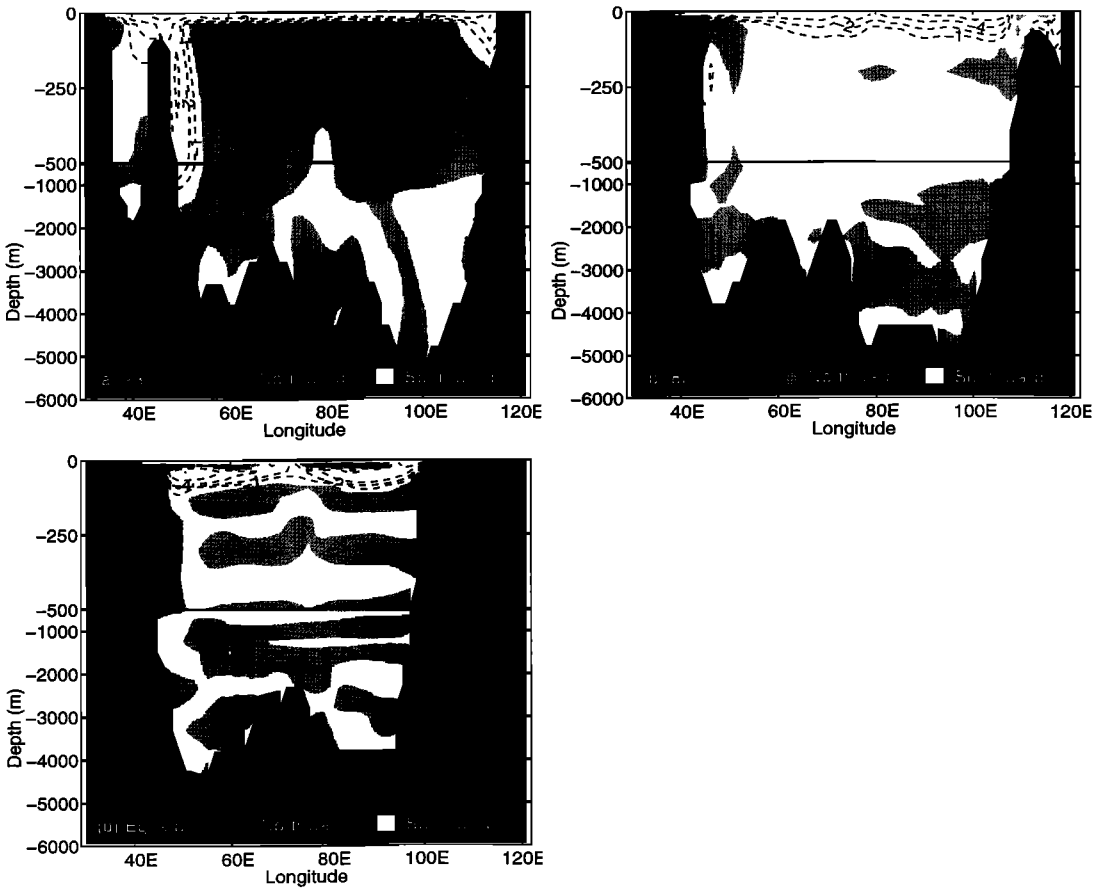

Figure 13. Meridional velocity sections at (a) 23°S, (b) 8°S, and (c) at the equator. Contour levels are −8, −4, −2, −1, 1, 2, 4, and 8 cm/s.

fluxes are turned off; in the second one, wind stress is turned off. Both model states are relatively well equilibrated after 10 years of integration. With wind forcing only, the subtropical front between 10° and 20°S is stronger, and the equatorial jet becomes both stronger and deeper (not shown). The meridional overturning (Figure 16a) is similar to that of run B, but the secondary circulations of the two currents are intensified. With buoyancy forcing only, the subtropical front and the equatorial jet both disappear, as do the secondary circulation cells (Figure 16b). The overturning is quite different from that with wind forcing only (or from that of run B); the dominant overturning pattern transports heat to the north.

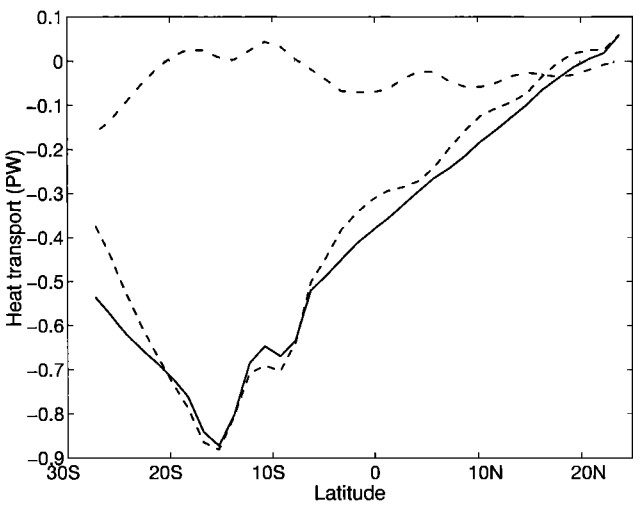

Figure 14. Total advective meridional heat transport (solid curve) and its two components associated with the vertical overturning (dashed curve) and horizontal circulation (dashed-dotted curve).

We conclude that the modeled meridional overturning of the Indian Ocean is primarily wind driven rather than by surface buoyancy forcing. Notice, however, the crucial role played by the lateral boundaries in setting up meridional transport.

5.2. Relative Versus Absolute Merit

We have shown that the solution of run B is better than those of the other experiments both statistically and physically. In this section we will present some detailed residual statistics of run B to investigate whether run B is a consistent solution. Attention is focused on the distribution of outliers as well as their causes and consequences; outliers are defined herein as grid points at which the absolute deviations of model temperatures from climatological values exceed two standard errors. If the process is Gaussian and observational errors at different grid points are uncorrelated as assumed, the outliers approximately represent grid points outside the 95% confidence interval. The number of outliers in any zonal, meridional, and horizontal plane is no more than a few percent of the total number of ocean grid points in the same plane. Thus run B is a satisfactory fit to climatological T and S.

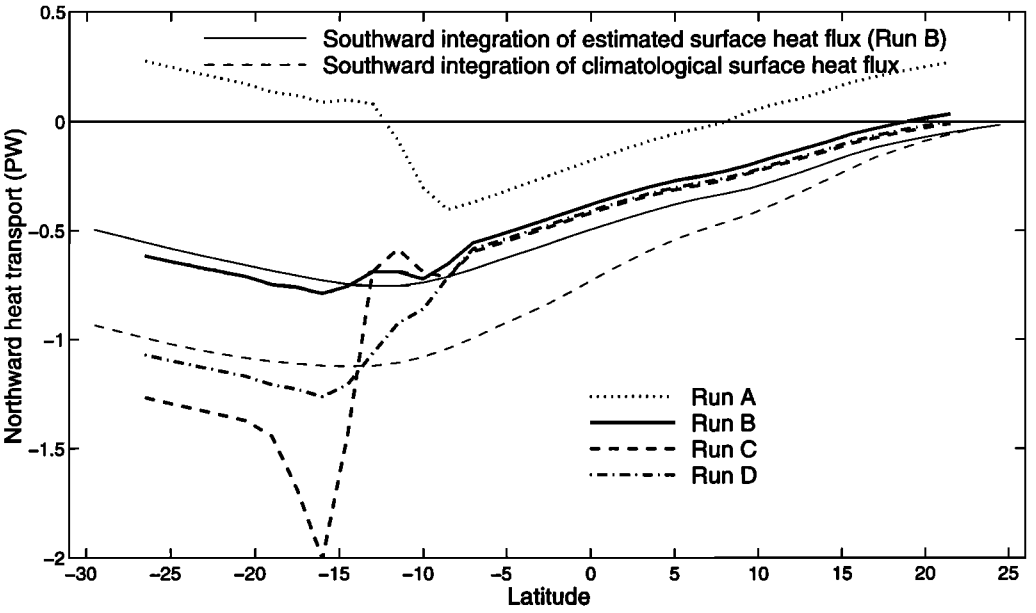

Figure 15. Meridional heat transports (thick curves) and surface heat fluxes integrated southward from the northern boundary (thin curves).

While the outliers tend to distribute randomly with longitudes and latitudes (not shown), they are concentrated in two depth ranges: in the upper 200 m (upper 6 levels) and between 2800 and 4300 m (levels 18–21) (Figure 17a). These points are all located near topography rather than in the interior. The deep outliers do not result in systematic deviations of model temperatures from climatology because, for each level, those that are warmer than climatology roughly equal those that are colder both in terms of the number of points and magnitude. However, the same is not true for the shallow outliers in the upper 200 m. They result in systematic deviations of model temperatures from climatology at different levels. Those in the first level (12.5 m) are all warmer than climatology; the opposite is true for those in levels 2–5 (37.5–125 m), and those in level 6 (200 m) are again warmer than climatology. Figures 17b, 17c, and 17d show the difference between model and climatological temperatures for levels 1, 4, and 6 along with the locations of outliers at each level. The horizontal advection of the anomalous temperatures of the outliers by flows at the corresponding levels (Figures 8a, 8b, and 8c) result in warmer, colder, and warmer temperatures for levels 1, 4, and 6, respectively.

The causes for the outliers may be related to several factors: (1) a possible lack of realistic mixing near some coastal regions and sharp topography at depth, (2) the smoothing procedure used to construct model topography and the subsequent mapping of the Levitus data onto model grids, and (3) the Levitus data were interpolated-extrapolated from hydrographic data (using an inverse-distance weighting method) so the derived climatological values near topography and in undersampled regions may be biased.

Although the shallow outliers lead to systematic deviations of interior temperatures from climatology and hamper a further reduction of model-data misfit, there is no evidence indicating that they are fundamental to the solution. In fact, the systematic deviations may be reduced or avoided by penalizing the gradient of model temperatures near the outlier locations. Therefore the residual patterns of model-data misfit do not preclude run B from being a consistent solution.

While the deep outliers do not cause a systematic model-data misfit, they might reflect the model's limitation in simulating enhanced vertical mixing near steep topography. The model is not configured to accommodate spatially varying mixing coefficients, but we examine the sensitivity of our solution to the overall value of vertical diffusivity. The optimization of run B is extended by changing the value of this coefficient from the original 0.3 to 1 cm^2/s. After 40 iterations the cost function, which initially increases by 20 times because of the change of vertical diffusivity, has been reduced back to a value close to that at the end of run B. The resultant overturning shows little change. Therefore our optimal solution is not very sensitive to the overall value of vertical diffusivity consistent with previous basin-scale inversions. In their review of the North Atlantic inversion, *Marotzke and Willebrand* [1996] suggest that the lack of deviation from advective balance in model fits to data is the cause for the insensitivity to vertical diffusivity. We have also performed a sensitivity experiment with respect to the horizontal diffusivity; the result is similar.

The temporal drift of the optimal solution is also evaluated in an extended forward integration following the optimization. When the solution of run B is integrated forward (with estimated surface fluxes and sponge conditions), little temporal drift occurs during a 300-year extended integration (a maximum of 3 Sv change in the overturning above 500 m near the equator). Therefore the optimal solution of run B can be used to initialize climate models of the Indian Ocean. We conclude that run B is an optimal steady state solution that is consistent with annual mean climatological data.

5.3. Role of Sponge Layers

This study illustrates the danger of using the conventional sponge layer as a side boundary condition commonly applied in regional modeling. In sponge layers, model temperatures and salinities are conventionally relaxed toward target values which

are fixed to either climatological values or hydrographic sections. Since the baroclinic mass exchange between a sponge and the model interior is set by the horizontal target density gradient through the thermal wind relation, errors in target values (deviations from annual averages caused by eddy, seasonal, and interannual signals as well as mapping and measurement errors) could render the flow field of the model interior unreliable. *Döscher et al.* [1994] found in a North Atlantic model that the interior flow field was improved by using a hydrographic section as targets T and S instead of climatology. This is not necessarily true in general because of the following. (1) A hydrographic section may contain eddy signals as well as seasonal to interannual variability and so may not be representative of the annual mean. Signal aliasing might be significant near the exits of the Agulhas and East Madagascar Currents; *Wunsch and Stammer* [1995], using altimetry data, observed large variabilities near that region even at periods shorter than 150 days. (2) Mapping error could be incurred by a mismatch between model and real topography; furthermore, one usually uses a "thick" sponge layer (i.e., one that has a thickness of several grid cells or more) so mapping a hydrographic section to one section within a thick sponge might not change the model state much.

Previous studies [*Holland and Bryan*, 1994; *Klinck*, 1995] have examined effects of using sponge layer (as opposed to physical open boundary condition) in a GCM of the Atlantic Ocean but have not addressed the role of errors in targets T and S. Even for forward models that use physical open boundary condition the inflow would still be affected by the bias in T and S at the open boundary. The estimation of targets T and S used in this study is a first, admittedly crude, attempt at open boundary estimation. This technique effectively eliminates the reverse overturning in the model interior and results in a much better solution.

Moreover, the sensitivity of the model solution to errors in targets T and S may depend on two factors. (1) A sponge layer might cross strong currents. In the present study the Persian Gulf and Red Sea sponges play a minor role as compared with the southern and the throughflow sponges. In particular, the southern sponge crosses two energetic western boundary currents (the Agulhas and East Madagascar Currents). Fluctuations associated with these currents could make a single hydrographic section unrepresentative of the annual averages and consequently force a regional model away from the true annual mean. (2) The "Ventilation" from the surface or from open boundaries has relative importance. In the North Atlantic, cold water masses are formed at high latitudes because of cooling and convection. In the Indian Ocean, however, cold water masses come from the Antarctic Circumpolar Current region. Therefore forcing by the southern boundary of the Indian Ocean might be more important than in the North Atlantic.

The sensitivity of model interior solution to targets T and S in the southern sponge deserves a few more words. The model state is sensitive to the target values in the southern sponge. This is why the prior estimates taken from *Levitus* [1982], *Levitus and Boyer* [1994], and *Levitus et al.* [1994] climatologies result in overturnings that have different strengths (although in the same direction), and the optimal estimates of target values in run B reverses the wrong overturning of run A. However, the solution of run B, our optimal solution, is not sensitive to the prior estimates of target values. The final estimates of target values for different prior estimates (*Levitus* [1982], *Levitus and Boyer* [1994], *Levitus et al.* [1994], or *Toole and Warren* [1993] section mapped to model grid) are very close because they are estimated from interior data in a dynamically consistent way. The strong sensitivity of the model state to the southern boundary conditions indicates that the latter can be estimated accurately if the model interior is well constrained by data. Conversely, if the model state is not sensitive to boundary conditions, the latter cannot be estimated accurately.

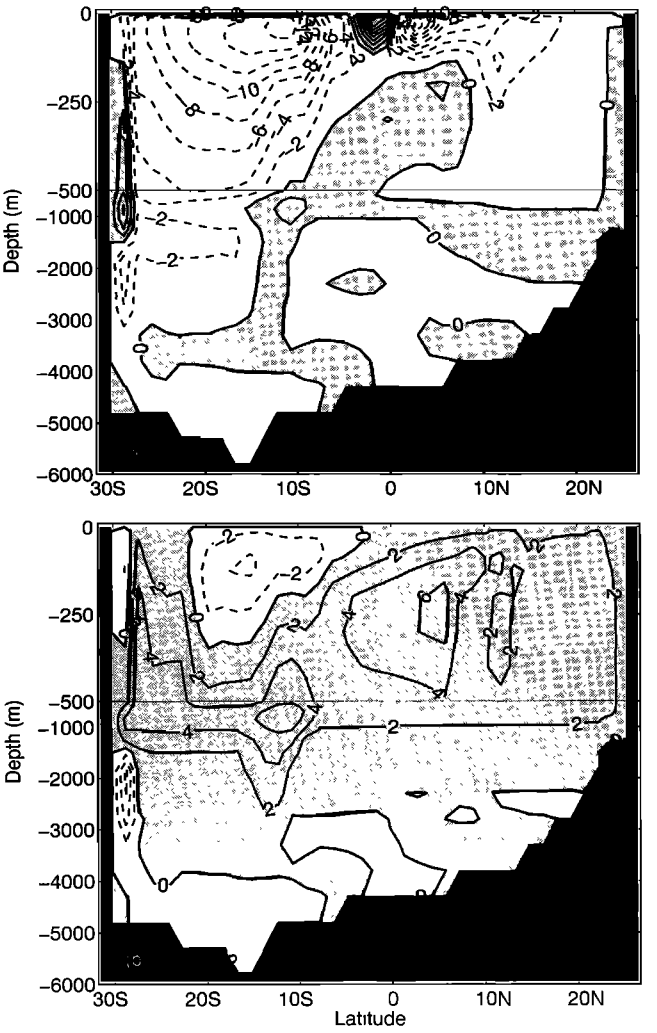

Figure 16. Meridional transport stream functions resulting from forward integration from the end product of run B, forced by (a) wind only and (b) buoyancy fluxes only.

One might be concerned that the smooth data [*Levitus and Boyer*, 1994; *Levitus et al.*, 1994] have reduced horizontal density gradients associated with deep currents. However, a model fit to the smooth data can sharpen the estimated horizontal density gradients. Examples of this are many; one of which being that the estimated zonal density gradients associated with the Deep Western Boundary Current against the Madagascar Ridge is larger than of the Levitus data. The same is true for the Agulhas, East Madagascar, and Leeuwin Currents. In their North Atlantic inversion, *Marotzke and Wunsch* [1993] also found that the model fit was able to sharpen density structures of the data. Producing a more dynamically consistent estimate of hydrography is actually one of the main purposes of model-data synthesis.

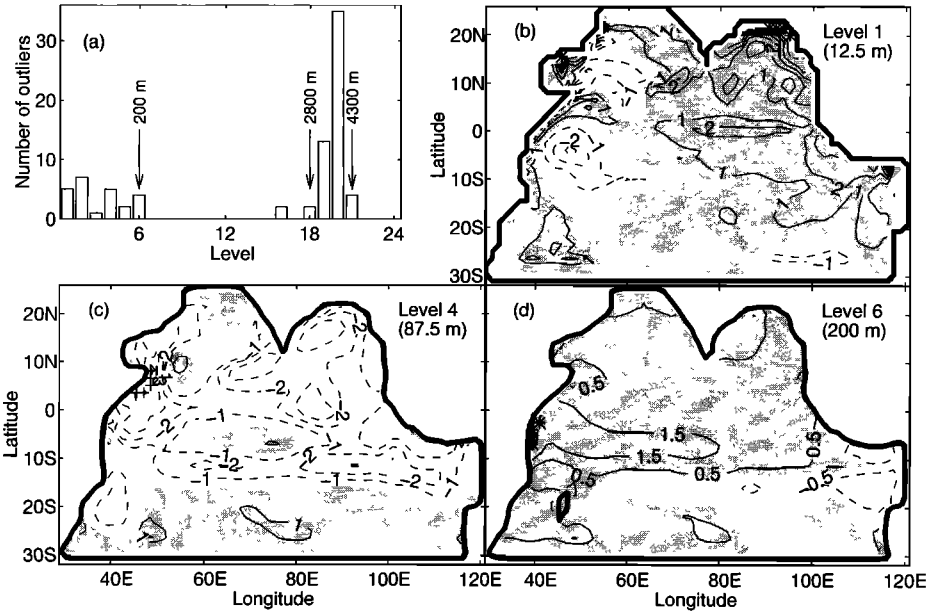

Figure 17. (a) Vertical distribution of outliers and model-data differences of temperature in °C at levels (b) 1, (c) 4, and (d) 6. Locations of outliers at each level are marked by asterisks and pluses representing warm and cold outliers, respectively.

5.4. Rectification by Seasonal Forcings

We have shown in section 3 that a forward integration with seasonal (side and surface) boundary forcings results in an annual average overturning that is similar to that of the forward integration with annual mean forcings. This also applies to the optimization experiments; the overturning of run B is similar to the annual average overturning resulting from an optimization in which monthly targets T and S in sponge layers and monthly surface forcings are estimated (not shown). The apparent lack of rectification by seasonal forcings is perhaps surprising.

In a steady inversion of the North Atlantic circulation, *Marotzke and Wunsch* [1993] suggested that the absence of a seasonal cycle may be the cause for the colder SST bias in the model fit to climatology. This is tied to the deep winter mixed layer in the North Atlantic and renders the concept of a dynamically consistent annual mean state invalid in the North Atlantic. The seasonal cycle in the Indian Ocean is much larger than that of the Atlantic, but there is no local deep water formation in the Indian Ocean. Hence the dynamics of the tropical Indian Ocean appears more linear than that of the North Atlantic which involves the highly nonlinear deep convection process. Therefore the experience of *Marotzke and Wunsch* [1993] with the North Atlantic inversion does not necessarily apply in the Indian Ocean. Furthermore, our near-surface horizontal circulation and meridional overturning in the upper few hundred meters are similar to the annual averages obtained by *McCreary et al.* [1993] using a 2½ layer model with seasonal forcings. This confirms that the lack of seasonal rectification in the Indian Ocean may be due to linear dynamics; the short adjustment time of our model indicates a dominant role of wave dynamics. There are many issues related to the seasonal cycle itself which are beyond the present scope and will be presented in a separate paper.

5.5. Sensitivity to Initialization

To examine the sensitivity of the solution of run B to different prior estimates of initial condition, two alternative experiments (of run B) are performed, which are initialized with the end products of runs C and D, respectively. These two states correspond to deep inflows of 20 and 10 Sv (see Figures 10a and 12a) in contrast to the outflow of 18 Sv for the standard initialization derived from 1 year of forward integration. In the following these two experiments are denoted by runs Bc and Bd, respectively. The cost functions in both experiments level out after 60 iterations. The final values of the cost function are about 3–5% lower than that using the standard initialization (i.e., the 1-year spinup state). This is primarily due to smaller temporal drifts. The total model-data misfits of T and S, however, is actually 7–8% larger. Therefore the resultant states are further away from the Levitus data than that obtained from run B using the standard initialization.

The resultant meridional transport stream functions (Figure 18) have strengths of 10 and 4 Sv at depth for runs Bc and Bd. Although the strength is different, there are several common features. (1) The optimization decreases the strength of the initial overturning (from 20 to 10 Sv for run Bc and from 10 to 4 Sv for run Bd). (2) The dominant overturning remains in the upper 1000 m. (3) There is little interior upwelling at depth; the deep inflows in both cases go into the throughflow sponge and upwell there like run C. For run Bc this results in very large vertical shear at depths near the throughflow area, inconsistent with throughflow observations. On the basis of approximate one-dimensional advective-diffusive balance as discussed in section 4.1 (run C), the 10 Sv of flow in and out of the throughflow sponge resulting from run Bc implies a vertical diffusivity as large as 500–1000 cm^2/s near the throughflow region. Therefore initialization from a state that has a large deep inflow results in an unrealistic solution in that area. In

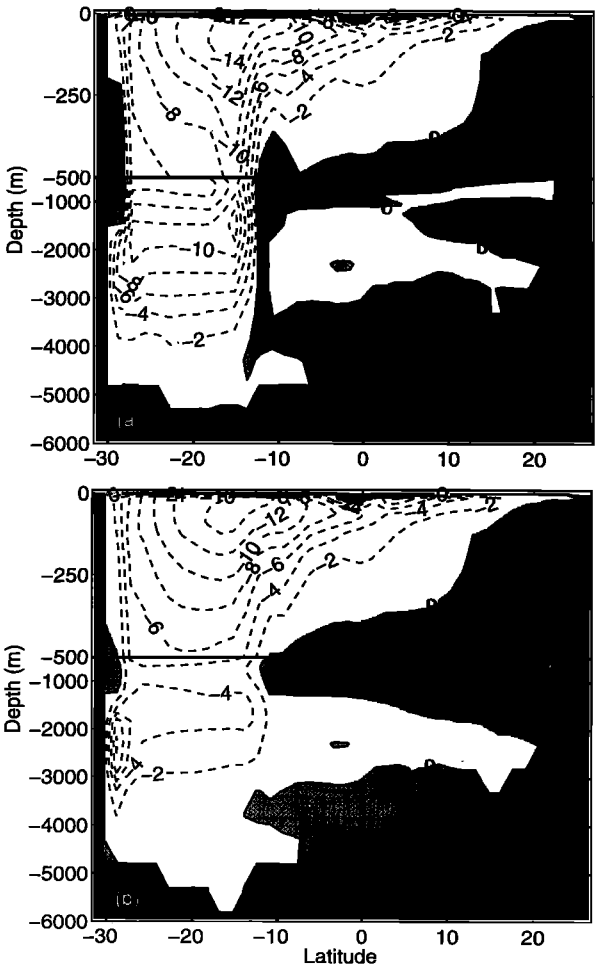

Figure 18. Meridional transport stream function resulting from sensitivity experiments of run B initialized from the end state of (a) run C and (b) run D, respectively.

comparison, the final state of run Bd has a more realistic vertical shear near the throughflow region. The southward heat transport of run Bd is very close to that of run B north of the throughflow region but is about 0.1 PW stronger south of the throughflow channel.

We have experimented with very different prior estimates of initial conditions, with the strength of overturning spanning approximately ±20 Sv. Although the estimated strength of deep inflow shows a moderate sensitivity (2–10 Sv), the dominant overturning remains in the upper 1000 m. Moreover, interior upwelling at depth remains weak. A moderately large deep inflow (order of 10 Sv) does not lead to a stronger interior upwelling but results in an unrealistic vertical shear structure near the throughflow region.

6. Concluding Remarks

This study represents the first attempt in a regional GCM to estimate the properties of open boundaries, albeit in a crude form: targets T and S in sponge layers are estimated as part of the optimization of the model state. As a result of the optimization of initial state, side boundary properties, and surface forcings, an optimal state of the Indian Ocean is found that is nearly steady while being consistent with climatological annual mean hydrography. The estimated surface heat gain is systematically smaller than climatological surface heat flux by amounts that are within observational uncertainty.

The meridional overturning obtained from the optimal solution is dominated by a shallow cell (<1000 m) of 14 Sv strength, with nearly uniform interior upwelling in the upper few hundred meters. The estimated net inflow from the Southern Ocean into the Indian Ocean at depth is weak. While the estimated magnitude of deep inflow into the Indian Ocean is moderately sensitive to the prior estimate of initial conditions, the estimated interior upwelling at depths is weak regardless of the initialization. Requiring a large net northward transport at depth into the Indian Ocean does not result in deep upwelling in the interior but leads to an unrealistic model state in that the baroclinic mass exchange and vertical mixing near the Indonesian throughflow region are much too large.

Admittedly, our estimated deep overturning might be somewhat too weak because of model errors (one of which being the absence of a net mass flux across the throughflow channel and the southern boundary). However, an inflow as large as 27 Sv estimated by *Toole and Warren* [1993] causes an inconsistency between the model and the data. The revised estimate by *Robbins and Toole* [1997], 10 Sv, is closer to our estimate.

Examination of the relative importance of wind and buoyancy forcings in maintaining the optimal model state indicates that surface wind stress is more important than surface buoyancy forcing in driving the meridional overturning of the Indian Ocean. *Robbins and Toole* [1997] found that only one third of their estimated 10 Sv deep inflow into the Indian Ocean upwells to the thermocline. This implies a lack of demand by surface buoyancy gain to bring up cold water at depth to maintain the upper ocean thermal balance, which is consistent with our finding that surface buoyancy gain is not the dominant driving mechanism. Our estimated overturning in the upper ocean, driven by wind, is stronger than the estimated deep overturning by *Robbins and Toole* [1997]. The lack of interior upwelling in our solution might well be consistent with their finding because the deep inflow they infer could be thought to upwell not in the interior but in the small throughflow region because of enhanced vertical mixing.

The present study does not address the effect of a net mass transport from the Pacific into the Indian Ocean via the Indonesian throughflow region (and consequently a net mass transport out of the southern boundary). This effect will be investigated by implementing open boundary estimation and is left for future study. Although the absence of the net mass flux is a clear model error, we do find a solution that is consistent with climatological temperatures and salinities in the interior as well as in the open boundaries (sponge layers). In other words, it is one possible solution. Moreover, even if the presence of a net mass flux causes a stronger deep overturning, our conclusion about the relative importance of surface wind and surface heat flux in driving the overturning is likely to remain valid.

Acknowledgments. We are indebted to Bob Long, S. M. Hwang, and Carlisle Thacker who constructed the prototype of the adjoint code to the GFDL model. Special thanks are due to Lisan Yu who made an improved version of the adjoint code available to us. This work was supported by grant OCE-930135 from the National Science Foundation. The computations were performed on Cray-YMPs at the National Center for Environmental Prediction and the National Center for Atmospheric Research, which is supported by the National Science Foundation.

References

Bergamasco, A., P. Malanotte-Rizzoli, W. C. Thacker, and R. B. Long, The seasonal steady circulation of the Eastern Mediterranean determined with the adjoint method, *Deep Sea Res., Part II, 40*, 1269–1294, 1993.

Cox, M. D., A primitive equation, 3-dimensional model of the ocean, *Ocean Group Tech. Rep. 1*, Geophys. Fluid Dyn. Lab./Princeton Univ., Princeton, N. J., 1984.

Döscher, R., C. W. Boning, and P. Herrmann, Response of circulation and heat transport in the North Atlantic to changes in thermohaline forcing in northern latitudes: A model study, *J. Phys. Oceanogr., 24*, 2306–2320, 1994.

Fieux, M., C. Andrie, P. Delecluse, A. G. Ilahude, A. Kartavtseff, F. Mantisi, R. Molcard, and J. C. Swallow, Measurements within the Pacific-Indian Oceans throughflow region, *Deep Sea Res., Part I, 41*, 1091–1130, 1994.

Fu, L.-L., Mass, heat and freshwater fluxes in the south Indian Ocean, *J. Phys. Oceanogr., 16*, 1683–1693, 1986.

Gates, W. L., and A. B. Nelson, A new (revised) tabulation of the Scripps topography on a 1 degree global grid, II, Ocean depths, *Rep. R-1277-1-ARPA*, Rand Corp., Santa Monica, Calif., 1975.

Hellerman, S., and M. Rosenstein, Normal monthly wind stress over the world ocean with error estimates, *J. Phys. Oceanogr., 13*, 1093–1104, 1983.

Holland, W. R., and F. O. Byran, Sensitivity studies on the role of the ocean in climate change, in *Ocean Processes in Climate Dynamics: Global and Mediterranean Examples*, edited by P. Malanotte-Rizzoli and A. R. Robinson, *NATO ASI Ser., Ser. C, 419*, 1–437, 1994.

Klinck, J. M., Thermohaline structure of an eddy-resolving North Atlantic model: The influence of boundary conditions, *J. Phys. Oceanogr., 25*, 1174–1195, 1995.

Levitus, S., Climatological atlas of the world ocean, *NOAA Prof. Pap. 13*, U. S. Govt. Print. Off., Washington, D. C., 1982.

Levitus, S., and T. P. Boyer, *World Ocean Atlas 1994*, vol. 4, *Temperature: NOAA Atlas NESDIS 4*, U. S. Dep. of Commer., Washington, D. C., 1994.

Levitus, S., R. Burgett, and T. P. Boyer, *World Ocean Atlas 1994*, vol. 3, *Salinity: NOAA Atlas NESDIS 3*, U. S. Dep. of Commer., Washington, D. C., 1994.

Macdonald, A., Oceanic fluxes of mass, heat, and freshwater: A global estimate and perspective, Ph.D. dissertation, 326 pp., Mass. Inst. of Technol., Cambridge, 1995.

Marotzke, J., The role of integration time in determining a steady state through data assimilation, *J. Phys. Oceanogr., 22*, 1556–1567, 1992.

Marotzke, J., and J. Willebrand, The North Atlantic mean circulation: Combining data and dynamics, in *The Warm Water Sphere of the North Atlantic Ocean*, edited by W. Krauss, pp. 55–90, Borntraeger, Berlin, 1996.

Marotzke, J., and C. Wunsch, Finding the steady state of a general circulation model through data assimilation: Application to the North Atlantic Ocean, *J. Geophys. Res., 98*, 20,149–20,167, 1993.

McCreary, J. P., Jr., P. K. Kundu, and R. L. Molinari, A numerical investigation of dynamics, thermodynamics and mixed-layer processes in the Indian Ocean, *Prog. Oceanogr., 31*, 181–244, 1993.

Meyers, G., R. J. Bailey, and A. P. Worby, Geostrophic transport of Indonesian throughflow, *Deep Sea Res., Part I, 42*, 1163–1174, 1995.

Oberhuber, J. M., *An Atlas Based on the COADS Data Set: The Budgets of Heat, Buoyancy and Turbulent Kinetic Energy at the Surface of the Global Ocean*, 100 pp., Max-Plank-Inst. fur Meteorol., Hamburg, Germany, 1988.

Robbins, P. E., and J. M. Toole, The dissolved silica budget as a constraint on the meridional overturning circulation of the Indian Ocean, *Deep Sea Res., Part I*, in press, 1997.

Semtner, A. J., Jr., and R. M. Chervin, Ocean general circulation from a global eddy-resolving model, *J. Geophys. Res., 97*, 5493–5550, 1992.

Sheinbaum, J., and D. L. T. Anderson, Variational assimilation of XBT data, Part I, *J. Phys. Oceanogr., 20*, 672–688, 1990.

Smedstad, O. M., and J. J. O'Brien, Variational data assimilation and parameter estimation in an equatorial Pacific Ocean model, *Prog. Oceanogr., 26*, 179–241, 1991.

Thacker, W. C., and R. B. Long, Fitting dynamics to data, *J. Geophys. Res., 93*, 1227–1240, 1988.

Toole, J. M., and M. E. Raymer, Heat and fresh water budgets of the Indian Ocean revisited, *Deep Sea Res., Part A, 32*, 917–928, 1985.

Toole, J. M., and B. A. Warren, A hydrographic section across the subtropical south Indian Ocean, *Deep Sea Res., Part I, 40*, 1973–2019, 1993.

Tziperman, E., W. C. Thacker, R. B. Long, and S. M. Hwang, Oceanic data analysis using a general circulation model, I, Simulations, *J. Phys. Oceanogr., 22*, 1434–1457, 1992.

U. S. World Ocean Circulation Experiment, *U. S. Contribution to WOCE Core Project 1: The Program Design for the Indian Ocean*, 80 pp., U. S. World Ocean Circ. Exp. Off., College Station, Tex., 1993.

Wacongne, S., and R. Pacanowski, Seasonal heat transport in a primitive equations model of the tropical Indian Ocean, *J. Phys. Oceanogr., 26*, 2666–2699, 1996.

Warren, B. A., Driving the meridional overturning in the Indian Ocean, *Deep Sea Res., Part I, 41*, 1349–1360, 1994.

Wunsch, C., The general circulation of the North Atlantic west of 50°W determined from inverse methods, *Rev. Geophys., 16*, 583–620, 1978.

Wunsch, C., and D. Stammer, The global frequency-wavenumber spectrum of oceanic variability estimated from TOPEX/POSEIDON altimetric measurements, *J. Geophys. Res., 100*, 24,895–24,910, 1995.

Yu, L., and P. Malanotte-Rizzoli, Analysis of the North Atlantic climatologies using a combined OGCM/adjoint approach, *J. Mar. Res., 54*, 867–913, 1996.

T. Lee, MS 300-323, Jet Propulsion Laboratory, California Institute of Technology, 4800 Oak Grove Drive, Pasadena, CA 91109. (e-mail: tlee@pacific.jpl.nasa.gov)

J. Marotzke, 54-1514, Center for Global Change Science, Massachusetts Institute of Technology, 77 Massachusetts Avenue, Cambridge, MA 02139.

(Received January 31, 1996; revised January 10, 1997;
accepted January 16, 1997.)